

Hot Carrier Transportation Dynamics in InAs/GaAs Quantum Dot Solar Cell

Tomah Sogabe,^{1,2,3,a)} Kohdaai Nii,² Katsuyoshi Sakamoto,² Koichi Yamaguchi,^{1,2} and Yoshitaka Okada³

¹⁾*i-Powered Energy Research Center (i-PERC), The University of Electro-Communications, Tokyo, Japan*

²⁾*Department of Engineering Science, The University of Electro-Communications, Tokyo, Japan*

³⁾*Research Center for Advanced Science and Technology (RCAST), The University of Tokyo, Tokyo, Japan*

(Dated: 3 December 2024)

The hot carrier dynamics and its effect on the device performance of GaAs solar cell and InAs/GaAs quantum dot solar cell (QDSC) was investigated. At first, the fundamental operation feature of conventional hot carrier solar cell was simulated based on the detailed balance thermodynamic model. Then we investigated the hot carrier dynamics in the normal junction based solar cell using hydrodynamic/energy Boltzmann transportation model (HETM) where the two temperature (carrier temperature and lattice temperature are treated separately. For the first time, we report an inherent quasi-equivalence between the detailed balance model and HETM model. The inter-link revealed here addresses the energy conservation law used in the detailed balance model from different angle and it paves a way toward an alternative approach to curtail the selective contact constraints used in the conventional hot carrier solar cell. In simulation, a specially designed InAs/GaAs quantum dot solar cell was used in the simulation. By varying the hot carrier energy relaxation time, an increase in the open circuit voltage was clearly found with the increase of. Detailed analysis was presented regarding the spatial distribution of hot carrier temperature and its interplay with electric field and three hot carrier recombination processes (Auger, SRH and Radiative)

Keywords: solar cell, quantum dot, hot carrier, dynamics, transportaion

^{a)}Electronic mail: sogabe@uec.ac.jp

I. INTRODUCTION

Hot carrier solar cell has drawn a lot of attentions due to its high theoretical efficiency limit of more than 80%^{1,2}. Conventionally, implementation of hot carrier solar cell requires (1) a photoactive material where cooling is slower than the transport to contacts; (2) a contact material which allows to selective extraction of electron or holes through a narrow energy band². Since this model is based on thermodynamics, it lacks of the interlink to the semiconductor device. Especially the implementation of selective contact in terms of semiconductor material is severely hindered due to the insufficient interpretation of the energy conservation thermodynamic constraints from the semiconductor device point of view. This is one of the main targets of the current work i.e. addressing the hot carrier operation principle from closed form of Boltzmann device transportation model.

In a typical bulk semiconductor device, cooling occurs in less than 10ps, while carrier extraction may take nanoseconds or longer. A lot of efforts have been devoted to slow the cooling process by well controlling the phonon scattering such as employing special bulk materials in which the energy coupling between phonon and electron could hardly occur. Recently, quantum well and quantum dot have also showed potentials to slow the hot carrier cooling rate³. An alternative way to slow down the cooling rate is to enhance the carrier separation rate. As having been reported in dye sensitized solar cell, an interfacial charge transfer can be fast and in less than a picosecond be exploited⁴. This is another target of current work: we focus on the investigation of the hot carrier separation/transportation dynamics in InAs/GaAs QDSC.

The paper is arranged as follows: 1) At first, the hot carrier solar cell operation principle was simulated based on the thermodynamic detail balance model containing a cooling and hot competing process. 2) A hydrodynamic model including the carrier energy w , where $w = \frac{3}{2}kT_H$ and T_H denotes the hot carrier temperature, was used to simulate a specially designed solar cell $GaAs_{n-emitter} | AlGaAs_{barrier} | GaAs_{intrinsic} | GaAs_{p-base}$. The results were compared with the simulation results using the drift-diffusion model (DDM) by varying internal electric field through adjusting GaAs intrinsic layer thickness, hot carrier relaxation time as well as the AlGaAs barrier thickness. 3) Detailed analysis regarding the spatial distribution of hot carrier temperature and the interplay with electric field and recombination was presented.

II. 'COOL' AND 'HOT' CARRIER COMPETING MODEL

Figure 1(a) shows the thermodynamic principle involving 'cool' and 'hot' competing dynamics. The hot carriers are assumed to reach a self-equilibrium between temperature and chemical potential. For a hot carrier solar cell, T_H and μ_H are competing with each other and are regulated based on the following equations¹:

$$\mu_{out} = \mu_H \left(\frac{T_a}{T_H} \right) \quad (1)$$

$$J = q \{ X f_s N(E_g, \infty, T_{sun}, 0) - N(E_g, \infty, T_{earth}, \mu_H) \} \quad (2)$$

$$J * E_{hot} = q \{ X f_s L(E_g, \infty, T_{sun}, 0) - L(E_g, \infty, T_{earth}, \mu_H) \} \quad (3)$$

where T_a is the ambient temperature and E_{hot} is the energy separation between the extracted electron and hole and in physics it equals to the kinetic energy; $N()$ is the photon flux density and $L()$ is the energy flux density, X and f_s are the parameters related to light

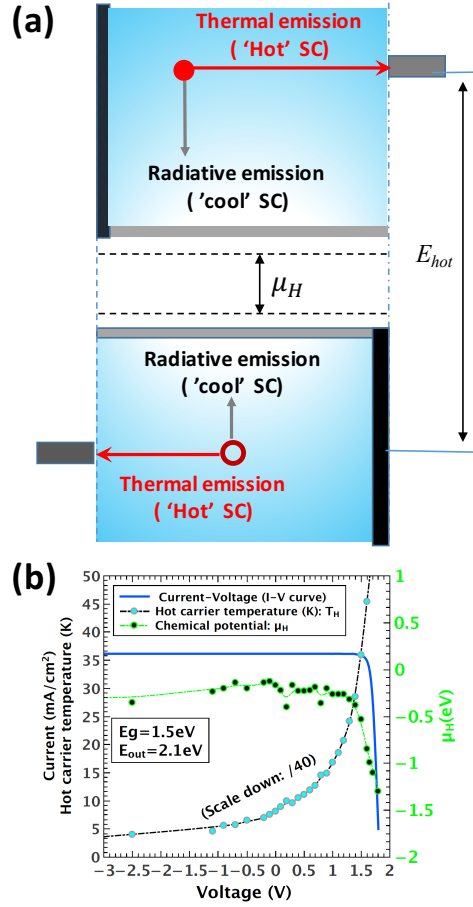


FIG. 1. (a) the sketch of the ‘cool’ and ‘hot’ competing process model. (b) Calculated results based on detailed balance principle together with energy conservation constraints. Here, $E_{hot} = 2.1\text{eV}$ and $E_g = 1.5\text{eV}$, $V = \frac{\mu_{out}}{q}$. note: T_H was scaled down by 40 to fit on the same figure.

concentration. If the hot carrier reaches the thermal equilibrium with ambient temperature T_a , then the hot carrier solar cell becomes the conventional solar cell and the output potential equals to $\mu_{out} = \mu_H$ (the quasi-Fermi level splitting). The J-V relation is derived by considering both the particle conservation (number of absorbed photons = number of emitted photons) described in equation (2) and the energy conservation in equation (3). Figure 1(b) shows the results of a hot carrier solar cell with bandgap $E_g = 1.5\text{eV}$ and the extraction energy separation E_{hot} was set at 2.1eV (note: this value can be varied to sort the maximum conversion efficiency). It is clearly seen here that by varying the output voltage $V = \frac{\mu_{out}}{q}$, the temperature of carriers T_H and chemical potential μ_H showed opposite trend indicating the competing behavior. As V increases, the output current decreases due to the increased photon emission which follows the Planck’s law $n(E) \approx E^2 \exp[-\frac{E - \mu_H}{kT_H}]$. Here we refer the photon emission controlled by μ_H as a ‘cool’ process and ones induced by temperature T_H as ‘hot’ process. The word ‘cool’ was so chosen as to reflect its similarity to the normal solar cell where the photo emission is solely controlled by chemical potential

μ because T_H is usually assumed to be constant as T_a . The word ‘cool’ was also chosen to reflect its value is much less than its counterpart in the normal solar cell and becomes zero or negative at the vicinity of V_{oc} . The existence of the ‘cool’ and ‘hot’ competition lies in the fact that for a hot carrier solar cell, it allows both μ_H and T_H to vary the number of emitted photons so as to reach the detailed balance with the totally absorbed photons. When V reaches the V_{oc} regime, the carrier temperature T_H increases dramatically while μ_H goes even to negative due to the stringent constraints of particle conservation and energy conservation. In other words, conventional solar cell at V_{oc} can be viewed approximately as an emitting diode at ambient temperature T_a while the hot carrier solar cell is exemplified as hot (high temperature T_H) thermal engine with μ_H being zero or even negative. as shown in the Figure 1(b).

III. HOT CARRIER DYNAMICS SIMULATION USING HYDRODYNAMIC / ENERGY TRANSPORTATION MODEL

After having investigated the competing dynamic behavior of the cool and hot carrier using the thermodynamic model, we further studied the hot carrier relaxation and extraction effect on solar cell device performance. This was implemented by converting the conventional DDM into the hydrodynamic model where the hot carrier energy $w = \frac{3}{2}kT_H$ was included. We have tackled this issue from two approaches: (i) a hydrodynamic model including hot carrier energy transportation using the commercial software, the Crosslight APSYS; (ii) extension of the self-developed DDM code to include the effects such as the electric field dependent mobility and diffusion coefficient as well as cooling and hot carrier competing dynamics illustrated in equation (1)⁵⁻⁷. The main formula used in approach (i) are given as follows⁸:

$$\nabla \cdot (\epsilon_c \nabla \psi) = -q(p - n + N_D^+ - N_A^-) \quad (4)$$

$$\frac{1}{q} \nabla \cdot J_n = -G + R \quad (5)$$

$$\frac{1}{q} \nabla \cdot J_p = G - R \quad (6)$$

$$\frac{J_n}{q} = \mu_n n \nabla \epsilon_c + D_n \nabla n + S_n \nabla T_{n,H} \quad (7)$$

$$\frac{J_p}{q} = \mu_p p \nabla \epsilon_c - D_p \nabla p - S_p \nabla T_{p,H} \quad (8)$$

$$\frac{\partial}{\partial t}(nw) + \nabla \cdot S - \frac{J_n}{q} \cdot \nabla \epsilon_c = \frac{\partial}{\partial t}(nw)|_c - w(R - G) \quad (9)$$

where the Here equation (4), (5), (6), (7), (8) are the familiar Poissons equation, current continuity equation and current density. Note that in (7) and (8), there is additional contribution to the current density due to the hot carrier temperature gradient when compared to the normal drift-diffusion simulation (DDM). These formulae are physically corresponding to the particle conservation equation (2) in thermodynamic detailed balance model. The key feature in hydrodynamic/energy transportation model is the energy balance equation (9). This equation, based some assumptions, can be simplified to a similar form of the energy conservation equation (3), as shown in Figure 2.

If we assume that in a conceptual thermodynamic device, it is reasonable to assume that

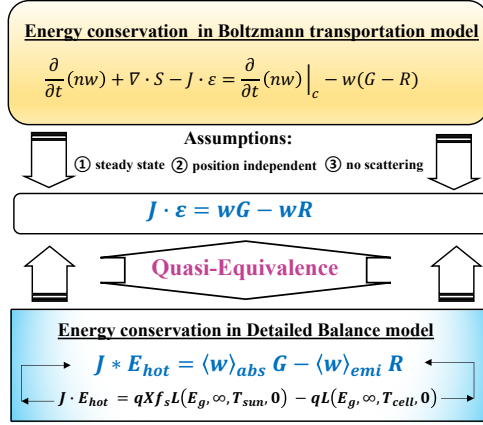


FIG. 2. Sketch of the derivation of quasi-equivalence between the energy conservation in detailed balance model and energy conservation in Boltzmann transportation model.

there is no position dependence, thus $\nabla \cdot S = 0$ and there is no scattering ($\tau_w \rightarrow \infty$) thus $\frac{\partial}{\partial t}(nw)|_c = 0$. Equation (9) can then be further simplified as:

$$J \cdot \varepsilon = wG - wR \quad (10)$$

Here ε is the electric field. Meanwhile, the formula (3) in the thermodynamic detailed balance model is rewritten so that the photon currents can be related to the energy currents via the average energies of the absorbed $\langle w_{abs} \rangle$ and emitted photons $\langle w_{emi} \rangle$ ⁹. These average photon energies are given by the absorbed or emitted energy currents divided by the appropriate photon currents G and R . The formula (3) was finally changed to:

$$J \cdot E_{hot} = \langle w_{abs} \rangle G - \langle w_{emi} \rangle R \quad (11)$$

As shown in Figure 2, it is apparent that a quasi-equivalence is built between the formula of (10) and formula (11). It is interesting to note that the most intriguing and challenging parameter in the thermodynamic model of hot carrier solar cell is the τ_w , which can be found corresponding exactly to the electric field ε , as shown in Figure 2. This indicates an alternative approach to implement the selective contact concept in semiconductor type hot carrier solar cell.

Figure 3 shows the simulated results where a specially designed solar cell $GaAs_{n-emitter} | AlGaAs_{barrier} | GaAs_{intrinsic} | GaAs_{p-base}$ was used as reference sample. A narrow n -type emitter was chosen and the intrinsic layer (i -GaAs) was set at 100nm to enhance the electric field effect. AlGaAs barrier was inserted between the i -GaAs and n -GaAs emitter to tune the hot carrier dynamics. The band diagram at thermal equilibrium and short circuit current J_{sc} as well as the open circuit voltage V_{oc} were illustrated in Figure 3(c) and 3(d). In order to further reveal the hot carrier transportation dynamics, energy dependent relaxation time τ_w was varied from $1 \times 10^{-14}s$ to $1 \times 10^{-11}s$ and the results were compared with those calculated by conventional DDM in which the hot carrier effect is ignored.

As it can be seen from 3(c), the J_{sc} tends to decrease with the increase of the relaxation time τ_w . We attributed the reduction of J_{sc} to the hot electrons induced current leak to the

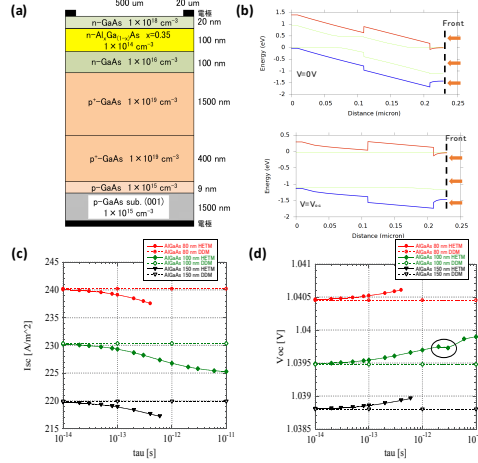


FIG. 3. Sketch of the derivation of quasi-equivalence between the energy conservation in detailed balance model and energy conservation in Boltzmann transportation model.

back electrode. An electron block layer acting as back surface field is expected to suppress the current reduction. Interestingly, we found that V_{oc} simulated under the HETM model showed much higher value than those simulated by DDM. Detailed analysis regarding its variation with τ_w will be given in the next section together with the interpretation of the hot carrier temperature distribution. In addition, the fill-factor (FF) was found improved in the hot carrier dynamics HETM simulation from 83.5% at $1 \times 10^{-14}s$ to 84.8% at $1 \times 10^{-11}s$. The FF increases with elongated carrier relaxation time indicating the enhanced carrier extraction under hot states, which will be discussed in more detail in the next section.

IV. DISCUSSION

A. Hot carrier temperature distribution

Figure 4 shows the hot carrier temperature distribution simulated using the HETM model by varying τ_w under a forward bias of 0.2V. The plot contains a $x-y$ plot of temperature distribution together with the 1-D band diagram of $E(x)$. We integrated the two plots in one plot to have a direct comparison between the electric field and hot carrier temperature.

It can be clearly seen from Figure 4(a) that extension of carrier relaxation time caused much higher carrier temperature and reached the highest value of more than 1200K when the τ_w is set as $1 \times 10^{-11}s$. We also found that the higher hot carrier temperatures were mostly distributed around junction area and the gradient gradually faded away the neutral region. Meanwhile, as shown in Figure 4(b), the hot carrier temperature showed strong dependence on the applied bias voltage. Forward bias voltage tends to diminish the temperature gradient. When the forward bias is greater than 0.9V, temperature of the carrier at the neutral region is found even below the lattice temperature (300K), indicating a cooling effect in the device. A quantitative analysis was presented to gain more deeper insight on the spatial distribution of the hot carrier temperature. If we define $\nabla \epsilon_c$ as the electric field ϵ , and the scattering term $\frac{\partial}{\partial t}(nw) |_c$ as: $-\frac{n}{\tau_w}(\frac{3}{2}kT_e - \frac{3}{2}kT_l)$, T_l and T_e are the lattice and electron temperature

respectively, then Formula (9) can be simplified as

$$\frac{1}{\tau_w} \left(\frac{T_l}{T_e} - 1 \right) = \frac{2}{3nkq} J_n \cdot \varepsilon - (G - R) \quad (12)$$

Here we have also ignored the term $\nabla \cdot S$. It can be seen that under this assumption, there exists a direct link between hot carrier temperature and the product of electron current and electric field $J_n \cdot \varepsilon$ as well as the net generation $(G - R)$. It is interesting to note that the contribution from $J_n \cdot \varepsilon$ is competing against the contribution from $(G - R)$. Phenomenologically, this can be understood as follows: while increasing the forward bias voltage, J_n and ε both decreases so its contribution to T_e decrease as well. On the other hand, with increase of the forward bias, the recombination R increases and the net generation rate $(G - R)$ decrease accordingly. Therefore its contribution to hot carrier temperature increases. Especially, when the device is under V_{oc} condition, thus $J_n = 0$ and equation (12) becomes:

$$\frac{1}{\tau_w} \left(1 - \frac{T_l}{T_e} \right) = G - R \quad (13)$$

In figure 4(b), we plotted both the spatial distribution of $J_n \cdot \varepsilon$ and ε together with the hot carrier temperature distribution under the applied external bias $V_{bias} = 0.2V$. It was found that the hot carrier temperature distribution was consistent with the electric field ε distribution while showed great deviation with the $J_n \cdot \varepsilon$. On the other hand, it was found that the hot carrier temperature distribution was strongly correlated with net generation $(G-R)$ when the external bias is at V_{oc} and the results was presented in figure 4(c). We also found the increase of hot carrier temperature with increase of relaxation time.i.e longer τ_w . All these results are consistent with equation (13). It is also important to mention that from Figure 4(c) , we speculate that it is the difference in $(G-R)$ between HETM and DDM simulation at V_{oc} induced the increase of V_{oc} in HETM simulation, as shown in Figure 3(d).

B. Hot carrier recombination behavior

In the HETM simulation, we have included the Auger, SRH and radiative recombination into the simulation. We found that for the device structure studied, SRH recombination prevails the other two. For instance, at $V_{appl} = 0.2V$, SRH: $\sim 10^{-8}/cm^3s$; Auger: $\sim 10^{-9}/cm^3s$ and Radiative: $\sim 10^{-10}/cm^3s$. Note that the recombination rate strongly depends on the applied bias voltage. HETM and DDM simulation. This means that SRH is the dominating recombination which has direct effect on the change of fill factor (FF). Detailed analysis results were given in Figure 5(a),(b),(c),(d), where the calculated three recombination dependence on the relaxation were given under forward bias of 0.9V. Meanwhile, for better understanding the hot carrier effect, we plotted the difference between HETM and DDM model. As can be seen from Figure 5, Auger, radiative and SRH recombination showed different tendency for the two models: HETM showed much higher value for Auger and radiative recombination than DDM but lower value for SRH recombination. It is also interesting to note that extending the relaxation time enhanced the tendency i.e. longer lifetime renders further higher value for Auger and Radiative recombination and further lower value for SRH recombination. Lower value of SRH at 0.9V is considered to contribute to the higher FF obtained from HETM simulation, as mentioned in previous section. It is worth to note that unlike the electric field, the spatial distribution profile for the three-recombination showed no consistence with the spatial distribution profile of hot carrier temperature. This is indicated by the dotted line shown in Figure 5, which shows that the SRH minimal position

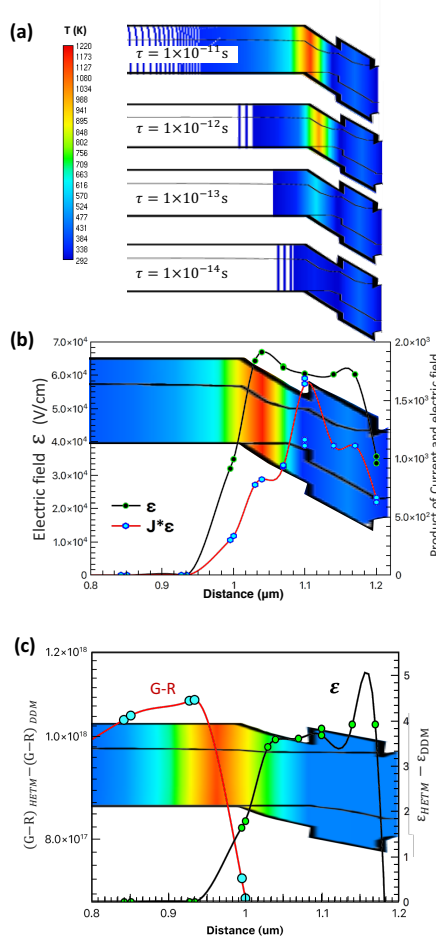


FIG. 4. (a) Carrier temperature distribution under different relaxation time; (b) Carrier temperature distribution together with the spatial distribution of electric field ϵ and the product of $J_n \cdot \epsilon$, the applied external voltage is 0.2V ; (c) Relation between the hot carrier temperature distribution and spatial distribution difference of net generation $(G - R)$ and electric field ϵ between HETM and DDM, the applied external voltage is V_{oc}

keeps constant for all the four types of relax times.

C. Increase of in HETM simulation

Here we gave a discussion about the increase of V_{oc} obtained from the HETM model from three different points of view:

1. Simplified J - V relation:

One simple approximation for the J - V relation two-temperature HETM can be made by taking the analogue of conventional one-temperature J - V model while inserting the temperature dependence for the related parameters. The formula can be approximated as:

$$V_{oc,HETM} \approx m(T_H)kT_H \ln \left\{ \frac{J_{sc}}{J_0(T_H)} + 1 \right\} \quad (14)$$

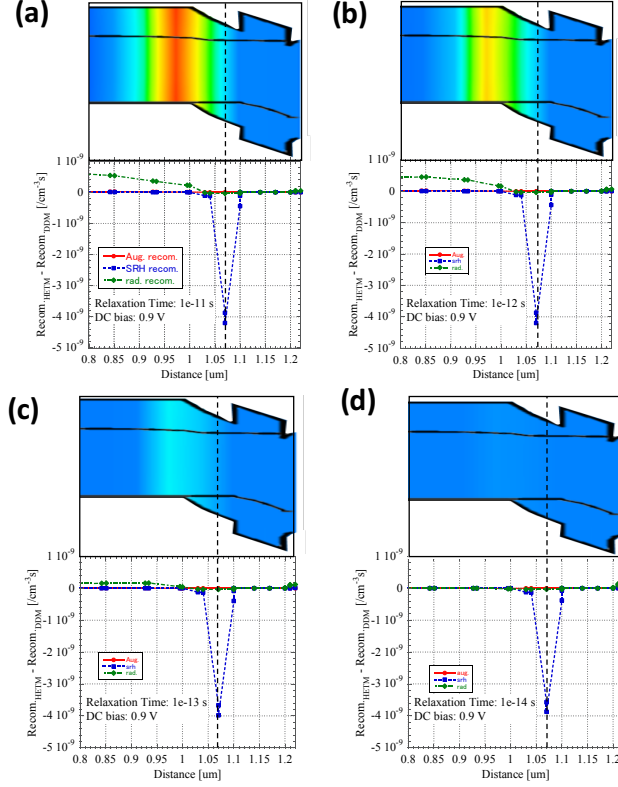


FIG. 5. Carrier temperature distribution under 0.9V and the Auger, SRH and radiative recombination for the carrier energy relaxation time (a) $1 \times 10^{-14} s$, (b) $1 \times 10^{-13} s$, (c) $1 \times 10^{-12} s$, (d) $1 \times 10^{-11} s$

where the $m(T_H)$ is the temperature dependent ideality factor; $J_0(T_H)$ is the temperature dependent recombination current, which corresponds to the SRH, Auger and radiative recombination mentioned previously. We have found that when at the V_{oc} , the J_0 calculated by HETM was higher than the ones by DDM. Meanwhile, the device temperature T_H is almost equal to so the only parameters which contribute to the increase of V_{oc} is the ideality factor $m(T_H)$. Based on a simple relation between FF and ideality factor derived by Green¹⁰, increase of FF calculated by using the HETM should be originated from a decrease of ideality factor. From the analysis above, we found the formula (14) failed to interpret the increase of V_{oc} calculated by using the HETM. In other words, a simplified J-V diode model is not applicable to analyze the HETM results.

2. Energy conservation analysis:

In principle, the difference between the DDM and HETM is the applied energy conservation law shown in the formula (9). The increase of V_{oc} should be fully understood through the closed form of formula (9). At V_{oc} , the current $J_n = 0$, formula (9) then reduced to formula (13). This is very significant result for understanding the HETM model. We found $(R - G)$ is depending on the carrier temperature and relaxation time. Although further investigation

is needed to gain deeper insight on this issue, net generation of (G-R) is considered to be the most decisive factor which altered the value of V_{oc} in the HETM simulation.

3. *Thermodynamic analysis:*

We can also address the increase of V_{oc} from an alternative thermodynamic point of view. As described in equation (1) and Figure 1(b), when a hot carrier solar cell is approaching its V_{oc} , the carrier temperature $m(T_H)$ will increase which will inevitably cause the reduction of μ_H . However, in our current simulation model, since we have not yet included the carrier separation term E_{hot} as designed in Figure 1, the V_{oc} represented here will be only controlled by the first half of the equation (1): $\mu_H(\frac{T_a}{T_H})$. If the T_H is higher than the T_a , μ_H has to increase to compensate the drop due to the increase of carrier temperature. This can be considered as the reason for the increased V_{oc} observed here and will decrease in a normally operated hot carrier solar cell assuming the E_{hot} can be correctly incorporated into the current hydrodynamic and energy transportation model. In addition, it is worthwhile to mention that the increases in can be converted to evaluate the hot carrier temperature and will be investigated in our future work.

Our further investigation will be focused on the competing principle in formula (12) between the net generation (G-R) and the product of $J_n \cdot \varepsilon$. We will compare this competing principle with the competing behavior between 'hot' and 'cool' process in the thermodynamic detailed balance model. Meanwhile, in current work, we have ignored the analysis regarding the energy flux $\nabla \cdot S$ and will be given full investigation regarding its effect on V_{oc} . Meanwhile, an InAs/GaAs QDSC will be fabricated based on the the simulated device structure to verify the hot carrier transportation effects by varying internal electric field as well as the AlGaAs barrier height.

D. CONCLUSIONS

Hot carrier dynamics in GaAs based solar cell was studied by using HETM by varying the hot carrier relaxation time and the results were compared to those simulated by using DDM. It was found that the J_{sc} tends to decrease with the increase of hot carrier relaxation time and showed lower value in the energy transport model than the DDM model. The V_{oc} , on the contrary, showed much higher value and which was analyzed based on both thermodynamic model and energy conservation in HETM simulation. Detailed analysis regarding the carrier temperature distribution and its relation to the electric field and net generation (G-R) were presented. Lastly increase of V_{oc} was interpreted in different models and found that the net generation (G-R) is possibly the key element. Simulations are undergoing by including the InAs QD into the current simulation model. Meanwhile experimental characterization of InAs/GaAs QDSC will be used to further examine the simulation results.

ACKNOWLEDGMENTS

We wish to acknowledge the financial support from the New Energy and Industrial Technology Development Organisation (NEDO) and to the Ministry of Economy, Trade and Industry (METI), Japan

REFERENCES

- ¹J.Nelson, *The Physics of Solar Cells* (Imperial College Press, London, 2003).
- ²P. Würfel, Sol. Energy Mater. Sol. Cells **46**, 43 (1997).
- ³A. Nozik, Ann. Rev.Phys.Chem. **52**, 193 (2001).
- ⁴A. Hagfeldt and M. Graetzel, Acc.Chem.Res **33**, 269 (2000).
- ⁵T. Sogabe *et al.*, Sci. Rep. **4**, 4972 (2015).
- ⁶S. Tomić, T. Sogabe, and Y. Okada, Prog. Photovolt: Res. Appl. **23**, 546 (2014).
- ⁷T. Sogabe, T. Kaizu, Y. Okada, and S. Tomić, J.Renew. Sustain. Ener. **6**, 011206 (2014).
- ⁸E. Azoff, IEEE Trans. ED **36** (1989).
- ⁹P. Würfel, A. Brown, T. Humphrey, and M. A. Green, Prog. Photovolt: Res. Appl. (2015).
- ¹⁰M.A.Green, Solid-State Electronics **24**, 788 (1981).